Relativistic Effects in Au L X-Ray Production by 0.5–3.0-MeV Protons*

G. A. Bissinger,† A. B. Baskin, B.-H. Choi, and S. M. Shafroth
University of North Carolina, Chapel Hill, North Carolina 27514
and Triangle Universities Nuclear Laboratory, Duke University, Durham, North Carolina 27706
and
J. M. Howard and A. W. Waltner
North Carolina State University, Raleigh, North Carolina
and Triangle Universities Nuclear Laboratory, Duke University, Durham, North Carolina 27706
(Received 18 January 1972)

Intensities and energies of gold $L\alpha$, $L\beta$, and $L\gamma$ composite x-ray peaks have been measured with a Si(Li) detector as a function of proton bombarding energies from 0.5–3.0 MeV. The ratios of $L\alpha/L\beta$ and $L\alpha/L\gamma$ peaks reach a maximum value at $E_p \approx 1$ MeV. An upward shift in the energy of the $L\gamma$ peak of ≈ 100 eV was observed at $E_p = 0.5$ MeV. Both effects (shifts and ratios) are due, at least in part, to the energy dependence of the L-subshell hole-production cross sections. The experimental results for the intensity ratios are in better agreement with theory if relativistic L-shell wave functions are used in the plane-wave Born-approximation calculations for L-subshell hole production.

The inclusion of relativistic wave functions in the plane-wave Born-approximation (PWBA) calculations of inner-shell ionization cross sections has been performed for the K shell[1] and L shell.[2] However, the necessity for consideration of relativistic effects in these calculations has not been clearly demonstrated due to the fact that in the total cross section these effects are important only for low-energy projectiles on high-atomic-number (Z) targets, where other corrections to these cross-section calculations, such as Coulomb deflection[3,4] and target-electron wave-function distortion by the finite charge of the incoming ion,[5] are also important.

The purpose of this paper is to point out that for high-Z targets, where recent theoretical work[2] indicates that relativistic effects will be quite important for L-shell ionization cross-section calculations, ratios of intensities of L x-ray peaks, viz.,

$$I_{L\alpha}/I_{L\beta} \text{ and } I_{L\alpha}/I_{L\gamma} \quad ,$$

are more nearly consistent with relativistic calculations and do not depend sensitively on Coulomb deflection effects. Furthermore, the trend of the observed shifts in energies of L x-ray peaks, particularly $L\gamma$ vs E_p, can be understood on the basis of relativistic L-subshell hole-production cross-section calculations.

The formulas used to relate theoretical L-subshell hole-production cross sections and expected peak intensities for $L\alpha$, $L\beta$, and $L\gamma$ composite x-ray peaks (Fig. 1) are given below:

$$I_{L\alpha} = \{[n_1(f_{13}+f_{12}f_{23}) + n_2 f_{23} + n_3]\omega_3\} F_{3\alpha} \quad , \tag{1}$$

$$I_{L\beta} = n_1\omega_1 F_{1\beta} + (n_1 f_{12} + n_2)\omega_2 F_{2\beta} + [n_1(f_{13}+f_{12}f_{23}) + n_2 f_{23} + n_3]\omega_3 F_{3\beta} \quad , \tag{2}$$

$$I_{L\gamma} = n_1\omega_1 F_{1\gamma} + (n_1 f_{12} + n_2)\omega_2 F_{2\gamma} \quad , \tag{3}$$

where $n_3 = 1$ and

$$n_1 = \sigma_{L1}/\sigma_{L3} \, , \qquad n_2 = \sigma_{L2}/\sigma_{L3} \, . \tag{4}$$

The ω_i and f_{ij} are the fluorescence and Coster-Kronig yields[6] for the various L subshells. The quantity $F_{3\alpha}$ is the fraction of radiative transitions

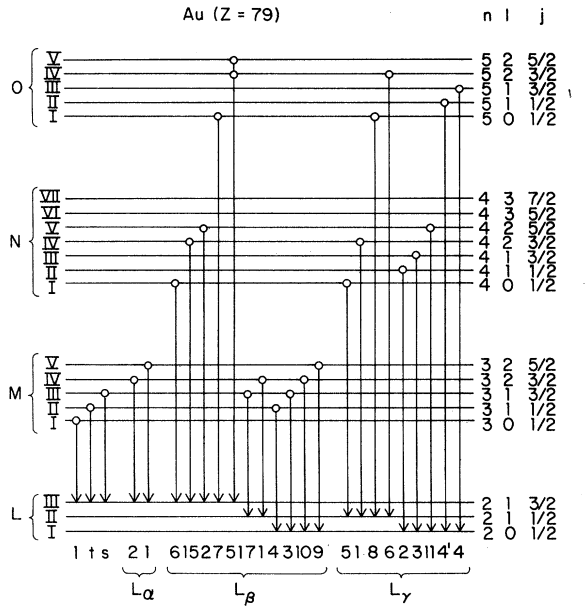

FIG. 1. Schematic energy-level diagram for Au showing the origins of the $L\alpha$, $L\beta$, and $L\gamma$ x-ray groups.

in the $L\alpha$ group which are associated with filling a hole in the $L3$ subshell, i.e.,

$$F_{3\alpha} = \Gamma_{3\alpha}/\Gamma_3 ; \quad (5)$$

Γ_3 is the sum of radiative widths for transitions which contribute to the L line that are associated with filling the hole in the $L3$ subshell. These radiative widths were taken from the calculations of Scofield.[7] The quantities $F_{1\gamma}$, $F_{2\beta}$, $F_{2\gamma}$, etc. are calculated in a similar manner. The theoretical $L\alpha/L\beta$ and $L\alpha/L\gamma$ ratios are just the ratios of the theoretical normalized intensities for $L\alpha$, $L\beta$, and $L\gamma$.

The theoretical values for σ_{L1}, σ_{L2}, and σ_{L3} will have quite similar corrections for Coulomb deflection since for a hydrogenlike atom the $2s$ and $2p$ subshells have rms radii within 20% of one another[8] (the $2p_{1/2}$ and $2p_{3/2}$ subshells have the same radial wave functions and electron-density distributions). The fact that Eqs. (1)–(3) all use ratios of these theoretical subshell cross sections will then cancel most of the Coulomb deflection corrections. Similarly, it is expected that distortion of the L-electron wave functions by the incident proton will be shared by all the subshells and that this effect too will cancel at least partially.

The experimental $L\alpha/L\beta$ and $L\alpha/L\gamma$ ratios for Au were derived from measurements made with a Si(Li) detector capable of resolving the $L\alpha$, $L\beta$, and $L\gamma$ lines produced by the 0.5–3.0-MeV-proton beam from the Triangle University Nuclear Lab 4-MeV Van de Graaff, incident on a target of ~30-μg/cm^2 gold evaporated onto a 20-μg/cm^2 C foil backing. These ratios cancel out target-thickness variations and current integration and minimize the effects of detector solid angle and relative photopeak detection efficiencies (the energy range for the $L\alpha$-$L\gamma$ lines is ~4 keV in a region where relative detection efficiency varies quite slowly). Energy loss in the target was ~3 keV and was neglected. The experimental set up is similar [except for the inclusion of a Si(Li) detector] to that reported previously.[9]

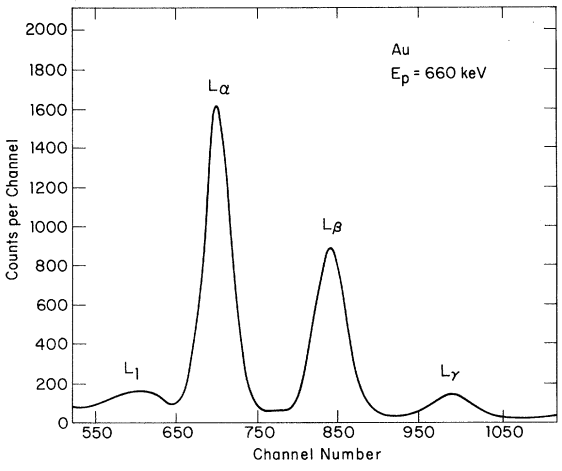

FIG. 2. Au L x-ray spectrum at a proton energy of 0.66 MeV.

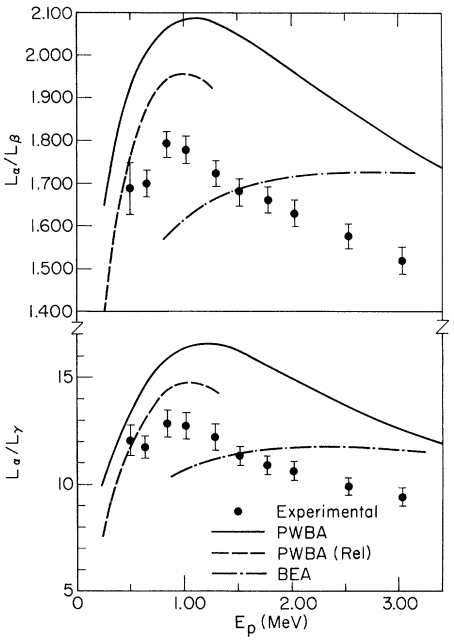

FIG. 3. $L\alpha/L\beta$ and $L\alpha/L\gamma$ ratios for proton energies from 0.5–3.0 MeV. [These ratios have been corrected for relative photopeak detection efficiencies, but the errors shown for these ratios do not include errors in the relative detection efficiencies, since this error (5%) would mask the actual relative behavior of these ratios.]

A typical L x-ray spectrum resulting from 0.66-MeV-proton bombardment of Au is shown in Fig. 2. The ratios $L\alpha/L\beta$ and $L\alpha/L\gamma$ as a function of beam energy and their values, experimental and theoretical, over the entire 0.5–3-MeV range are shown in Fig. 3. The PWBA results are derived from tabulated values[10] of σ_{L1}, σ_{L2}, and σ_{L3}, while the binary-encounter-approximation (BEA) results are derived from those for Mg K-shell ionization by protons using the method described in Ref. 4. The latter work permits calculation of cross sections corrected or uncorrected for Coulomb deflection. Use of the calculations without Coulomb deflection incorporated did not change the BEA predictions for $L\alpha/L\beta$ and $L\alpha/L\gamma$ ratios by more than 1%. This substantiates the earlier statement that ratios of L-subshell ionization cross sections cancel this Coulomb deflection effect. The relativistic PWBA subshell cross-section calculations have been reported elsewhere[11] by one of us (B.-H. C).

It is clear that inclusion of relativistic wave functions in the PWBA calculations produces

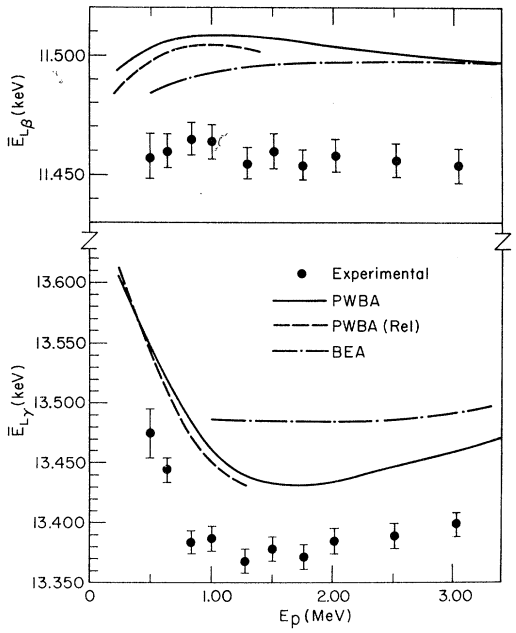

FIG. 4. The centroid shifts in $L\beta$ and $L\gamma$ for proton energies from 0.5–3.0 MeV.

a substantial improvement in the agreement between theory and experiment, for the $L\alpha/L\beta$ and $L\alpha/L\gamma$ ratios. Unfortunately these theoretical calculations are not available for $E > 1.25$ MeV because of convergence difficulties at higher energies. However the theoretical curve is accurate over the energy range shown in Fig. 3.

Also associated with the relative variation in L-subshell hole-production cross sections is a beam-energy-dependent shift in the centroid position for the Au $L\beta$ and Au $L\gamma$ lines which are composite lines with contributions from at least two subshells. Such a shift has been observed in this experiment for $L\gamma$. The energy shifts expected for $L\beta$ are at the limits of detectability with the present Si(Li) detector, and no shift is expected for $L\alpha$ since it involves only the $L3$ subshell, and none is observed. The centroid energies for $L\beta$ and $L\gamma$ for 0.5–3.0-MeV protons are presented in Fig. 4. The PWBA theory predicts a minimum in the $L\gamma$ centroid energy near 1.7 MeV which is in rough agreement with experiment. The BEA curve for $\bar{E}_{L\gamma}$ shows only an ~ 20-eV energy shift for proton energies from 1–30 MeV while experimental results over this region (this work and Ref. 12) indicate energy shifts in $L\gamma$ in excess of 100 eV. The relativistic PWBA calculations unfortunately do not extend far enough in energy to reproduce this minimum, although over the restricted region of these calculations, the agreement with experiment is slightly better than the nonrelativistic PWBA calculation.

The centroid energy for $\bar{E}_{L\gamma}$, for example, is given by

$$\bar{E}_{L\gamma} = [n_1\omega_1 F_{1\gamma}\bar{E}_{1\gamma} + (n_1 f_{12} + n_2)\omega_2 F_{2\gamma}\bar{E}_{2\gamma}]/L\gamma , \quad (6)$$

where $\bar{E}_{1\gamma}$ and $\bar{E}_{2\gamma}$ are the centroid energies for contributions from the $L1$ and $L2$ subshells to $L\gamma$. The centroid associated with the $L1$ subshell is calculated from (7),

$$\bar{E}_{1\gamma} = \sum_i \Gamma_{\gamma_i} E_{L\gamma_i} / \sum_i \Gamma_{\gamma_i} , \quad (7)$$

where the $E_{L\gamma_i}$ are the energies (taken from the compilation by Bearden[13]) of the components of $L\gamma$ which originate from the $L1$ subshell. The Γ_{γ_i} are the radiative widths associated with these transitions.

The fact that $L\alpha$ does not exhibit a shift seems to rule out the multiple inner-shell ionization mechanism in the present case since this effect would give rise to observable shifts of 20–30 eV per L hole.

In summary, the inclusion of relativistic wave functions for the target atom in the PWBA calculations of $L\alpha/L\beta$ and $L\alpha/L\gamma$ ratios gives improved agreement with experimental $L\alpha/L\beta$ and $L\alpha/L\gamma$ intensity ratios and agrees with the trend of the centroid shifts in the $L\beta$ and $L\gamma$ lines. These ratios, which are relatively free from Coulomb deflection, distortion of target atom wave functions by the finite proton charge, binding of the target electron to the projectile and other effects, demonstrate the necessity of inclusion of relativistic effects in calculations of the inner-shell ionization cross sections for high-Z atoms. The pronounced energy shift in $L\gamma$ while $L\alpha$ shows no shift is further evidence that the explanation lies in the hole-subshell cross-section ratio variation with bombarding energy.

---

†Present address: Physics Department, Rutgers University, New Brunswick, N. J. 08903.

*Work supported by U. S. Atomic Energy Commission.

[1]D. Jamnik and C. Zupancic, Kgl. Danske Videnskab. Selskab, Mat.—Fys. Medd. 31, No. 2 (1957).

[2]B.-H. Choi, Phys. Rev. A 4, 1002 (1971).

[3]J. Bang and J. M. Hansteen, Kgl. Danske Videnskab. Selskab, Mat.—Fys. Medd. 31, No. 13 (1959).

[4]J. D. Garcia, Phys. Rev. A 1, 280 (1970).

[5]G. Basbas, W. Brandt, R. Laubert, A. Ratkowski, and A. Schwarzschild, Phys. Rev. Letters 27, 171 (1971).

[6]R. W. Fink, R. C. Jopson, H. Mark, and C. D. Swift, Rev. Mod. Phys. 38, 513 (1966).

[7]J. H. Scofield, Phys. Rev. 179, 9 (1969).

[8]L. Pauling and E. B. Wilson, *Introduction to Quantum Mechanics* (McGraw-Hill, New York, 1935), p. 144.

[9]G. A. Bissinger, J. M. Joyce, E. J. Ludwig, W. S. McEver, and S. M. Shafroth, Phys. Rev. A 1, 841

(1970).
[10]Recent revised calculation by one of us (B.-H. C.).
[11]B.-H. Choi, Bull. Am. Phys. Soc. 16, 1357 (1971).
[12]S. M. Shafroth, G. A. Bissinger, and A. W. Waltner (to be published).
[13]J. A. Bearden, Rev. Mod. Phys. 39, 78 (1967).

PHYSICAL REVIEW A VOLUME 6, NUMBER 2 AUGUST 1972

Construction of Projection Operators in the Semiclassical Approximation*

Yukap Hahn† and Kenneth M. Watson
Physics Department and Lawrence Berkeley Laboratory, University of California, Berkeley, California 94720
(Received 13 March 1972)

The projection operators onto various subsets of states of a quantum-mechanical system are constructed in a semiclassical approximation based on the Wigner transformation of statistical mechanics. As illustrations, explicit operator expressions are derived for the cases of central Coulomb potential, one-dimensional harmonic oscillator, and radial Coulombic states of specified angular momenta. The accuracy of these operators is then examined in some detail in terms of the overlap integrals and dipole transition probabilities. The semiclassical approximation is found to be effective in the energy regions away from the classical turning points. Extensions of the approach to partially projected Green's functions and other related moments are discussed and their applications to scattering problems pointed out.

I. INTRODUCTION

Projection operators occur frequently in formulations of theories of scattering reactions, such as that of Feshbach[1] and its subsequent developments.[2] For example, a calculation of compound resonance states may be set up in terms of the closed-channel operator Q which is orthogonal to all open channels at a given energy E. The variational bound formulation[3] of effective potentials and resulting bounds on reaction matrix elements is also developed with the use of projection operators.

The difficulty of constructing such projection operators has been an obstacle in the application of these theories. In this paper we describe the use of the Wigner[4] transformation of statistical mechanics to provide a semiclassical approximation for projection operators.

The Wigner transformation expresses the Boltzmann function as a certain Fourier transform of the quantum-mechanical density matrix. Applied to the case of the single-particle distribution function this relation is[5]

$$f(\vec{x},\vec{p}) = h^{-3}\int (\vec{x}-\tfrac{1}{2}\vec{r}\,|\,\rho\,|\,\vec{x}+\tfrac{1}{2}\vec{r})\,e^{i\vec{p}\cdot\vec{r}/\hbar}\,d^3r\ . \quad (1.1)$$

Here f is the Boltzmann function for a particle at $\vec{x}$ with momentum $\vec{p}$ and $(\vec{x}\,|\,\rho\,|\,\vec{x}')$ is the density matrix in a coordinate-space representation.[6] The inverse of (1.1) is

$$(\vec{x}\,|\,\rho\,|\,\vec{y}) = \int d^3p\, f\left(\tfrac{1}{2}(\vec{x}+\vec{y}),\vec{p}\right)e^{i\vec{p}\cdot(\vec{x}-\vec{y})/\hbar}\ . \quad (1.2)$$

The normalization in Eq. (1.1) is so chosen that

$$\int f(\vec{x},\vec{p})\,d^3x\,d^3p = \int d^3x\,(\vec{x}\,|\,\rho\,|\,\vec{x}) = 1\ , \quad (1.3)$$

when ρ is expressed in a Hilbert-space representation:

$$(\vec{x}\,|\,\rho\,|\,\vec{y}) = \frac{1}{M}\sum_{\alpha=1}^{M}\psi_\alpha(\vec{x})\,\psi_\alpha^\dagger(\vec{y})\ , \quad (1.4)$$

the average being over an appropriate ensemble with ψ_α, the wave function of α in that ensemble.

II. PROJECTION OPERATOR ONTO STATES OF ONE OR MORE PARTICLES

Relations (1.1), (1.2), and (1.4) suggest the application to projection-operator construction with a change in normalization, of course. Consider a complete set $\chi_\lambda(\vec{x})$ of orthonormal single-particle wave function. The projection operator onto a subset s of these is

$$(\vec{x}\,|\,\Lambda\,|\,\vec{y}) = \textstyle\sum_s \chi_\lambda(\vec{x})\,\chi_\lambda^*(\vec{y})\ . \quad (2.1)$$

A classical phase-space function $F(\vec{x},\vec{p})$ is introduced as[7]

$$F(\vec{x},\vec{p}) = \int (\vec{x}-\tfrac{1}{2}\vec{r}\,|\,\Lambda\,|\,\vec{x}+\tfrac{1}{2}\vec{r})\,e^{i\vec{p}\cdot\vec{r}/\hbar}\,d^3r\ . \quad (2.2)$$

The inverse transformation is

$$(\vec{x}\,|\,\Lambda\,|\,\vec{y}) = \frac{1}{h^3}\int F\left(\tfrac{1}{2}(\vec{x}+\vec{y}),\vec{p}\right)e^{i\vec{p}\cdot(\vec{x}-\vec{y})/\hbar}\,d^3p\ . \quad (2.3)$$

If the χ_λ are normalized to unity, the normalization of F is

$$\int F(\vec{x},\vec{p})\,d^3x\,d^3p = h^3\textstyle\sum_s\ . \quad (2.4)$$

Consider now the plane-wave states

$$\chi_{\vec{p}}(\vec{x}) = h^{-3/2}\,e^{i\vec{p}\cdot\vec{x}/\hbar}$$

in some large volume $\mathcal{V}$. The projection operator